RESEARCH ARTICLE

Metagenomic Assay for Identification of Microbial Pathogens in Tumor Tissues

Don A. Baldwin,[a,d*] Michael Feldman,[a,b] James C. Alwine,[a,c] Erle S. Robertson[a,b]

Abramson Cancer Center[a] and the Departments of Microbiology,[d] Pathology and Laboratory Medicine,[b] and Cancer Biology,[c] Perelman School of Medicine, University of Pennsylvania, Philadelphia, Pennsylvania, USA

* Present address: Don A. Baldwin, BioQuarry, Newtown Square, Pennsylvania, USA.

ABSTRACT **Screening for thousands of viruses and other pathogenic microorganisms, including bacteria, fungi, and parasites, in human tumor tissues will provide a better understanding of the contributory role of the microbiome in the predisposition for, causes of, and therapeutic responses to the associated cancer. Metagenomic assays designed to perform these tasks will have to include rapid and economical processing of large numbers of samples, supported by straightforward data analysis pipeline and flexible sample preparation options for multiple input tissue types from individual patients, mammals, or environmental samples. To meet these requirements, the PathoChip platform was developed by targeting viral, prokaryotic, and eukaryotic genomes with multiple DNA probes in a microarray format that can be combined with a variety of upstream sample preparation protocols and downstream data analysis. PathoChip screening of DNA plus RNA from formalin-fixed, paraffin-embedded tumor tissues demonstrated the utility of this platform, and the detection of oncogenic viruses was validated using independent PCR and deep sequencing methods. These studies demonstrate the use of the PathoChip technology combined with PCR and deep sequencing as a valuable strategy for detecting the presence of pathogens in human cancers and other diseases.**

IMPORTANCE **This work describes the design and testing of a PathoChip array containing probes with the ability to detect all known publicly available virus sequences as well as hundreds of pathogenic bacteria, fungi, parasites, and helminths. PathoChip provides wide coverage of microbial pathogens in an economical format. PathoChip screening of DNA plus RNA from formalin-fixed, paraffin-embedded tumor tissues demonstrated the utility of this platform, and the detection of oncogenic viruses was validated using independent PCR and sequencing methods. These studies demonstrate that the PathoChip technology is a valuable strategy for detecting the presence of pathogens in human cancers and other diseases.**

Received 7 August 2014 **Accepted** 8 August 2014 **Published** 16 September 2014

Citation Baldwin DA, Feldman M, Alwine JC, Robertson ES. 2014. Metagenomic assay for identification of microbial pathogens in tumor tissues. mBio 5(5):e01714-14. doi: 10.1128/mBio.01714-14.

Editor Michael J. Imperiale, University of Michigan Medical School

Address correspondence to Erle S. Robertson, erle@upenn.edu.

This article is a direct contribution from a Fellow of the American Academy of Microbiology.

In 2008, over 2 million cases of cancer worldwide (approximately 20% of all tumors) were associated with one of a number of infectious agents: 10 viruses (papillomavirus; hepatitis B and C viruses; polyomaviruses BK virus, JC virus, and Merkel cell polyomavirus [MCpyV]; Epstein-Barr virus [EBV]; human herpesvirus 8; T-cell leukemia virus type 1; and human T-cell leukemia virus type 2), one bacterium (*Helicobacter pylori*), and two helminths (schistosomes and liver flukes) which are major contributors to cancers as etiological agents (1). Considering the thousands of microbial species that comprise the normal human microbiome (2), it is likely that the microbe communities can substantially influence normal physiology, as well as the causes of (or major contributors to) and response to diseases (3), including cancer. These effects are the subject of intense investigation in tissue systems known to have resident microbiomes, which include the gastrointestinal tract (4–6), skin (7), and airway (8–10), and in immune and inflammatory responses (11–14). Microbiome profiling is also examining the less obvious roles for microbes and their presence in unexpected locations. Some examples that are relevant but not limited to cancer include modulation of tumor microenvironments (15) and dysbiosis of bacterial populations in breast cancer tissues (16).

As *de novo* cataloguing expands the count of microbial species in the human microbiome and characterizes their distributions, metagenomic tools are needed to efficiently identify an infectious agent strongly associated with a disease. The ability to evaluate the contributions of a microbiome will be necessary to understand the interactions between pathogens, pathogen interactions with commensal organisms, host genetics, and environmental factors.

PCR amplification using universal 16S rRNA primers, followed by amplicon sequencing, is the most widely used strategy for exploring investigations in associated microbiomes and provides an effective discovery tool (17). However, this will work only for bacterial species with amplicons that survive population PCR but not for viruses or eukaryotic microorganisms. 16S rRNA sequencing can also be used to screen large sets of samples but may

have difficulty in discriminating between strains or reporting the presence of genomic variants or pathogenicity factors. Deep sequencing of the total DNA from a sample can certainly identify bacterial, viral, and other microbiome members (3, 17, 18) but with a severe penalty in efficiency. Even if the field attains the as-yet-unrealized goal of a cost of $1,000 per genome, total DNA sequencing will be an expensive method for screening hundreds or thousands of experimental and control samples to detect associations of pathogens with a particular disease. Depending on the specimen sampled, the data may overwhelmingly be from host human sequences, creating an unnecessarily large search space for locating pathogen signatures and resulting in the majority of sequence reads being discarded.

DNA microarrays have been used for metagenomics. The Lawrence Berkeley Lab/Affymetrix PhyloChip is based on rRNA sequences (19). An academically developed Virochip has probes for 1,500-plus viruses (20, 38–44) and has successfully detected viruses in pathology samples. The Virochip platform is limited to viruses and assays RNA that is reverse transcribed to cDNA for PCR amplification (20, 38–44). The Glomics GeoChip 4.0 focuses on RNA expression by bacteria in the human microbiome (21) and covers bacteriophages but no other viruses, nor any eukaryotic microorganisms. PathGen Dx has launched a PathChip kit that features an Affymetrix microarray for all known viruses and a broad selection of bacteria (22) but no eukaryotic pathogens.

These and other array-based tools illustrate the demand for methods to quickly and economically screen sets of samples for broad microbial content, including species beyond bacteria (23). This report describes development of the PathoChip platform containing probes for all known publicly available virus sequences and hundreds of pathogenic bacteria, fungi, and helminths, providing wide coverage of microbial pathogens in an economical format. Where possible, multiple probes to independent regions of the target genome are used to improve an opportunity for detection. Furthermore, while the PathoChip content was developed from sequences to known targets, the ability to discover new strains or organisms is provided by the inclusion of probes to sequences that are conserved within and between viral families. To this end, a previously unknown virus with homology to a conserved sequence may produce a corresponding hybridization signal from such a probe, if not to a complete probe set. A supporting workflow is described for profiling large collections of tumor samples typically available as formalin-fixed, paraffin-embedded (FFPE) tissue in biobanks and includes simultaneous detection of DNA and RNA to expand the range of targets available for hybridization.

RESULTS

Microarray design. The PathoChip design goals were to cover all public NCBI viral genomes and genomic sequences from a broad selection of microorganisms (bacteria, fungi, and parasites) that are pathogenic to humans, using multiple probes to independent target sites in the genome of each species (Fig. 1A). The resulting collection of pathogen sequences was assembled into a metagenome containing 58 chromosomes of 448.9 million bp and 5,206 accessions for over 4,200 viruses, bacteria, fungi, and parasites. Agilent custom probe design algorithms built for comparative genomic hybridization applications were used to identify 5.5 million probes from the metagenome. Over 3 million of these probes were predicted to have low risk of cross-hybridization with a human genome sequence. Importantly, a subset of these probes that map to unique target regions of the selected pathogens was synthesized on PathoChip v2a microarrays, and a separate subset that covers regions of sequence conservation between at least two or more viruses was synthesized on PathoChip v2b arrays (Fig. 1B). An enhanced feature of the PathoChip v2b was the inclusion of 2,085 probes tiled throughout the lengths of 22 accessions for agents known to be tightly associated with human cancers.

Pilot assays using Agilent reference human DNA showed median probe intensities of over 750 fluorescence units for probes to human sequences, around 17 fluorescence units for nonhuman specific probes on PathoChip v2a, and 120 fluorescence units for nonhuman conserved probes on PathoChip v2b (experiment 1, Table 1). These assays identified 6,360 probes with fluorescence values of >150 that would apparently be able to hybridize to human DNA and were therefore removed from consideration for generation of the PathoChip v3 design, which combined the unique and conserved probe sets (Fig. 1B).

Pilot experiment 1 indicated that the presence or absence of Cot-1 DNA made no difference in probe performance (Tables 1 and 2). Therefore, this reagent was omitted from subsequent assays. Interestingly, very high hybridization intensities were noted for probes to Epstein-Barr virus (EBV; human herpesvirus 4) from this control human DNA. The manufacturer confirmed that cell lines used to prepare the male and female SureTag human reference DNA were infected with this virus to generate the cell lines. EBV detection in tumor screening assays that used this reagent was therefore possible if the signals were not normalized to EBV probe signals to the xhh Cy5 channel. Future assays for our screens utilized virus-free reference human DNA as the cross-hybridization control after validation through a number of stringent steps for detection of other known viruses.

Assay response to positive controls. The limited amounts of tissue available in most tumor archives or obtained from clinical procedures, such as fine needle aspirates and other biopsy specimens, require that metagenomic screening protocols include efficient strategies for nucleic acid extractions combined with an amplification step which allows for genome- or transcriptome-wide representation of microbial agents present in the sample. These methods must additionally be compatible with the degraded DNA and RNA typically produced by formalin tissue fixation. A draft workflow was designed to address these technical hurdles (Fig. 1C), and pilot experiments were conducted to test the amplification and detection of a number of positive-control viruses.

Three whole-genome amplification (WGA) methods that use phi29 polymerase rolling-circle amplification (24) (GenomiPhi), universal primer multiplex PCR (25) (GenomePlex and TransPlex), or single-primer isothermal amplification (26) (Ovation WGA) were tested for their ability to detect a small bacteriophage genome spiked into a background of human DNA (15 ng). phiX174 DNA at copy numbers 1×, 10×, and 100× relative to a single-copy human genomic locus was easily detected by PathoChip probes after any of the amplification reactions (Fig. 2A). To test detection of human DNA and RNA viruses, DNA from cell lines containing adenovirus type 5 or RNA containing respiratory syncytial virus was amplified by the GenomePlex DNA and TransPlex RNA methods (experiments 2 and 3, Table 2). The cell line DNA and RNA samples were then mixed and simultaneously amplified by TransPlex (experiment 4, Table 2). Probes for both viruses produced strong and specific

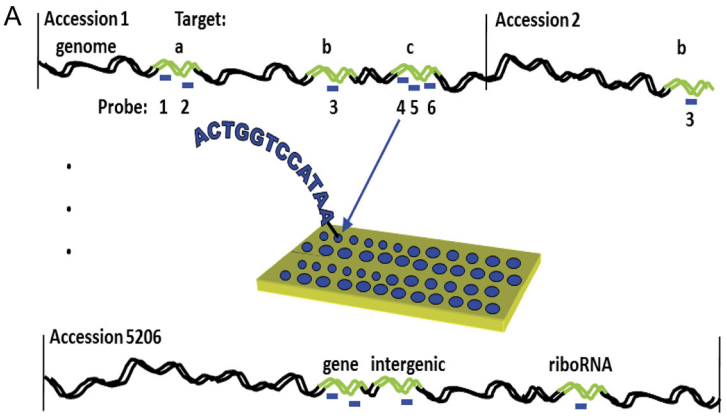
A
Accession 1
Target:
genome
a
b
c
Accession 2
b
Probe: 1 2
3
4 5 6
3
ACTGGTCCATAA
Accession 5206
gene
intergenic
riboRNA

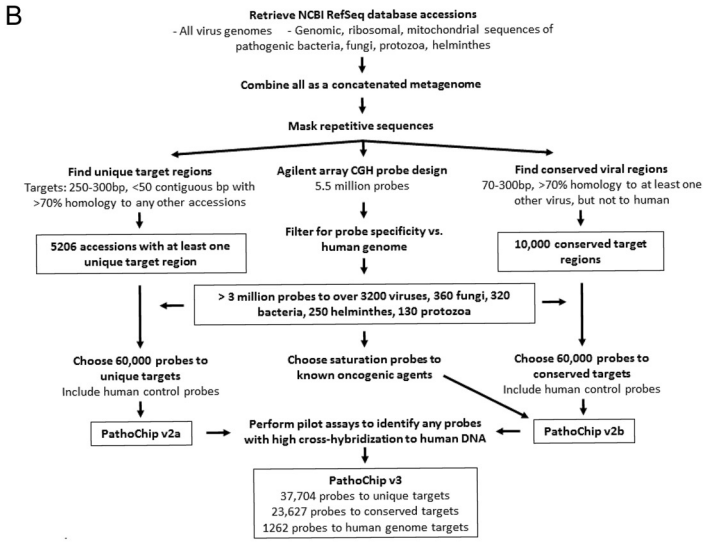
B
Retrieve NCBI RefSeq database accessions
- All virus genomes - Genomic, ribosomal, mitochondrial sequences of pathogenic bacteria, fungi, protozoa, helminthes
Combine all as a concatenated metagenome
Mask repetitive sequences
Find unique target regions
Targets: 250-300bp, <50 contiguous bp with >70% homology to any other accessions
Agilent array CGH probe design
5.5 million probes
Find conserved viral regions
70-300bp, >70% homology to at least one other virus, but not to human
5206 accessions with at least one unique target region
Filter for probe specificity vs. human genome
10,000 conserved target regions
> 3 million probes to over 3200 viruses, 360 fungi, 320 bacteria, 250 helminthes, 130 protozoa
Choose 60,000 probes to unique targets
Include human control probes
Choose saturation probes to known oncogenic agents
Choose 60,000 probes to conserved targets
Include human control probes
PathoChip v2a
Perform pilot assays to identify any probes with high cross-hybridization to human DNA
PathoChip v2b
PathoChip v3
37,704 probes to unique targets
23,627 probes to conserved targets
1262 probes to human genome targets

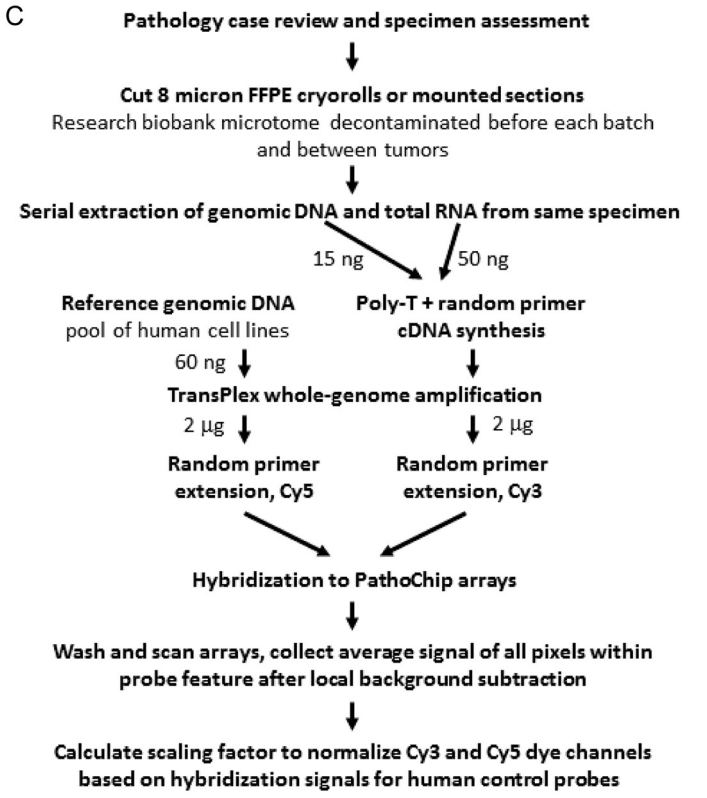
C
Pathology case review and specimen assessment
Cut 8 micron FFPE cryorolls or mounted sections
Research biobank microtome decontaminated before each batch and between tumors
Serial extraction of genomic DNA and total RNA from same specimen
15 ng
50 ng
Reference genomic DNA
pool of human cell lines
Poly-T + random primer cDNA synthesis
60 ng
TransPlex whole-genome amplification
2 µg
2 µg
Random primer extension, Cy5
Random primer extension, Cy3
Hybridization to PathoChip arrays
Wash and scan arrays, collect average signal of all pixels within probe feature after local background subtraction
Calculate scaling factor to normalize Cy3 and Cy5 dye channels based on hybridization signals for human control probes

TABLE 1 Pilot PathoChip assays with human and nonhuman probes

Expt	PathoChip	Test (Cy3)	xhh cross-hybridization control (Cy5)	Amplification	Fluorescence value[b]			
					Human probes		Nonhuman probes	
					Median Cy3	Median Cy5	Median Cy3	Median Cy5
1	v2a	Human gDNA,[a] no Cot-1	Human gDNA, no Cot-1	None	794	785	18	17
1	v2b	Human gDNA, no Cot-1	Human gDNA, no Cot-1	None	726	741	119	124
1	v2a	Human gDNA + Cot-1	Human gDNA + Cot-1	None	758	794	17	17
1	v2b	Human gDNA + Cot-1	Human gDNA + Cot-1	None	758	791	121	128
2	v2a	Adenovirus type 5 + host gDNA	Human gDNA	GenomePlex WGA	284	784	8	18
3	v2a	Respiratory syncytial virus + host DNA	Human gDNA	TransPlex WTA	448	825	10	16
4	v2a	Adenovirus type 5 + respiratory syncytial virus + host gDNA and RNA	Human gDNA	TransPlex WTA	371	832	7	15

[a] gDNA, genomic DNA.
[b] Relative fluorescence units.

detection signals. This indicated that the TransPlex reverse transcription worked robustly in the presence of genomic DNA, and genomic DNA and cDNA targets were coamplified.

Human adenovirus type 5, JC polyomavirus, or BK polyomavirus DNA was added to a background of 15 ng of human DNA at absolute copy numbers ranging from 10,000 to 10 viral genomes. After TransPlex amplification, adenovirus type 5 was detected by PathoChip probes at all copy numbers while the polyomavirus probes produced detectable signal above background, detecting at least 100 genome copies (Fig. 2B).

The genomic sequence of human cytomegalovirus (CMV) strain AD169, a laboratory-adapted strain, differs at several locations from the NCBI reference CMV sequence, a clinical strain. This includes a large deletion. DNA from a cell line infected with CMV AD169 was amplified and hybridized to PathoChip v3, which includes a set of saturation tiling probes for the CMV reference genome. While most probes produced high signals, probes located at sites that are polymorphic or deleted in CMV AD169 had significantly reduced fluorescence signals, clearly delineating the polymorphisms or deletions in the laboratory strain (Fig. 2C).

Assay performance with tumor tissue samples. The AllPrep DNA/RNA FFPE kit provides efficient extraction of genomic DNA and total RNA from the same FFPE specimen, so this kit was tested for its ability, importantly, to extract nucleic acids from fungal cells and Gram-negative or Gram-positive bacteria, which are likely to be the most difficult microbial agents in the samples. DNA and RNA from *Saccharomyces cerevisiae*, *Bacillus cereus*, and *Escherichia coli* cultures were efficiently recovered using the kit (data not shown). This provided a preliminary indication that nucleic acids from eukaryotic and prokaryotic pathogens can be extracted and detected from the PathoChip tumor extraction procedure (Fig. 1C).

The screen was performed on an initial set of eight oropharyngeal squamous cell carcinoma (OSCC)/head and neck carcinoma samples from FFPE tissue specimens. Human p16 overexpression from the CDKN2A gene is correlated with oncogenic human papillomavirus (HPV) infection in OSCC, and p16 immunohistochemistry is used as a prognostic molecular biomarker in clinical pathology laboratories, with high sensitivity but poor specificity for HPV (27). The OSCC samples included five p16-positive tumors and three p16-negative tumors as determined by pathology at the Hospital of the University of Pennsylvania. From our PathoChip screen, four of the five p16(+) tumors produced high detection signals across the 68 PathoChip probes for HPV16, and the fifth tumor showed signals for a small subset of HPV16 probes. The remaining tumors were negative for PathoChip HPV16 detection (Fig. 3). Despite good hybridization to other p16(+) samples, three of the HPV probes for tumor 2025 and two probes for tumor 2028 had no detectable signal This is suggestive of an HPV strain variation, which was similar to the results from polymorphic sites in the CMV positive-control experiment.

Development of PathoChip analysis strategies using OSCC tumor screening data. Oncogenic viruses may undergo significant genomic rearrangements or deletions in host tumors. Furthermore, viral strains can be widely polymorphic, and detection of a new pathogen may rely on signal from a single probe. Several levels of data analysis are therefore needed to detect three main classes of "hits" that might be expected in a screening project (Fig. 4). Accession signal (AccSig), the average of all probes for an accession adjusted for human DNA cross-hybridization, was calculated to screen for detection by a majority of probes in an accession's set. MAT (model-based analysis of tiling arrays) scores (28) from a sliding window of probes were calculated to detect local areas of high signal regardless of accession boundaries. *t* tests with multiple testing correction were employed at the individual probe level to identify probes with signal consistently higher than back-

FIG 1 PathoChip design and tumor screening workflow. (A) Sequence accessions for all viruses and selected human-pathogenic microorganisms were retrieved from the NCBI DNA sequence databases and concatenated to form a metagenome. Wherever possible, regions of target sequence unique to the accession (a and c) were used to select multiple 60-nt probes (1, 2, and 4 to 6) for microarray synthesis, and probes to target regions that share similar sequences in at least two viral accessions (b) were also identified. Probes to prokaryotic and eukaryotic pathogens may map to intergenic, gene, or rRNA sequences or a mixture of target types, depending on the availability of sequence data. (B) Parallel and iterative design processes were used to assemble the PathoChip probe collection that covers unique and conserved target regions, supplemented with high-resolution probe tiling for known cancer-associated microorganisms. (C) The PathoChip tumor screening protocol simultaneously assays DNA and RNA from small amounts of tissue recovered from formalin-fixed, paraffin-embedded (FFPE) tumor specimens.

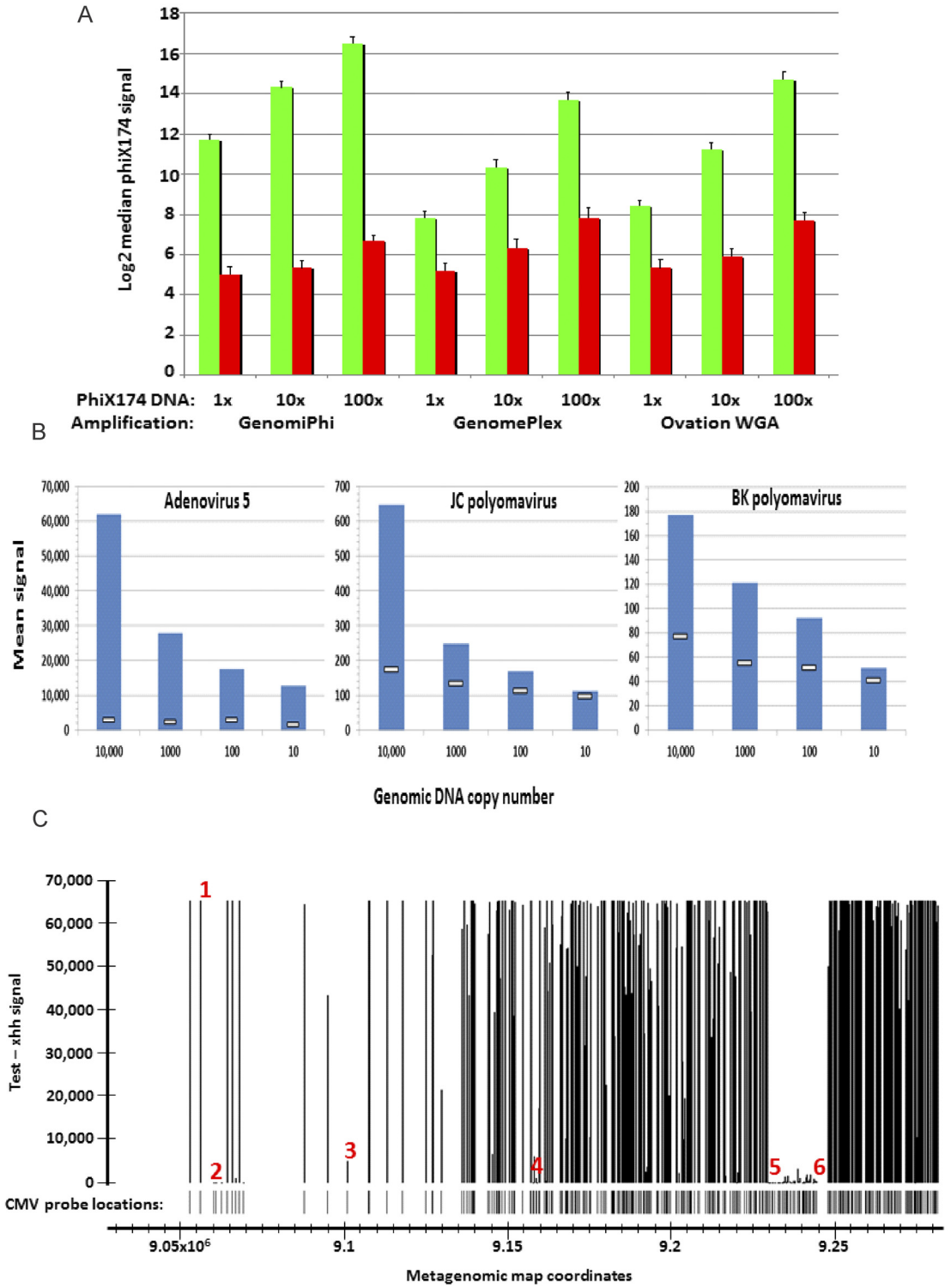

FIG 2 PathoChip assay performance assessed using positive-control DNA. (A) Whole-genome amplification kits that feature three different enzymatic processes were compared in their abilities to detect phiX174 bacteriophage genomic DNA spiked into human DNA. 1× DNA was equivalent to the molarity for a single-copy locus in the human genome. Green bars are the median Cy3 signal for the 14 phiX174 probes hybridized to test samples, and red bars show the median Cy5 signal from control samples (human DNA only). Error bars indicate standard deviations across probes. (B) Detection responses for three viruses were measured over a dilution series from 10,000 to 10 genomic copies per sample. Genomic DNA for each virus was spiked into a reference amount of human DNA. Blue bars are the average Cy3 signals for all probes to the indicated viruses hybridized to test samples, and white lines indicate the probes' Cy5 average from control samples (human DNA only). (C) Human cytomegalovirus (CMV) DNA was hybridized to a PathoChip containing 299 probes for saturation tiling across the reference CMV genome (NCBI accession NC_006273). The DNA was from CMV AD169, a strain that differs from the reference sequence at several locations, and was spiked into a background of human DNA for cohybridization with reference human DNA only (xhh). Red numerals indicate example probes for positive detection (1), low signal due to sequence polymorphisms (2, 3, and 4), and missing signal due to deletion in AD169 (5 and 6).

TABLE 2 Pilot PathoChip assays with virus

Expt	PathoChip	Test (Cy3)	xhh cross-hybridization control (Cy5)	Amplification	Fluorescence value[b]			
					Epstein-Barr virus		Adenovirus type 5 AccSig	Respiratory syncytial virus AccSig
					Median Cy3	Median Cy5		
1	v2a	Human gDNA,[a] no Cot-1	Human gDNA, no Cot-1	None	33,617	52,563	4	4
1	v2b	Human gDNA, no Cot-1	Human gDNA, no Cot-1	None	32,694	15,693	0	0
1	v2a	Human gDNA + Cot-1	Human gDNA + Cot-1	None	32,026	56,239	0	1
1	v2b	Human gDNA + Cot-1	Human gDNA + Cot-1	None	13,420	17,067	0	0
2	v2a	Adenovirus type 5 + host gDNA	Human gDNA	GenomePlex WGA	292	61,188	64,426	0
3	v2a	Respiratory syncytial virus + host DNA	Human gDNA	TransPlex WTA	281	63,036	0	49,161
4	v2a	Adenovirus type 5 + respiratory syncytial virus + host gDNA and RNA	Human gDNA	TransPlex WTA	196	63,495	64,218	30,793

[a] gDNA, genomic DNA.
[b] Relative fluorescence units.

ground across the population of tumors, and an outlier analysis was conducted for probes with high signal but only in one or a few tumors from the screening population.

Data from a screening project of 100 OSCC tumors were used to evaluate these analysis methods. AccSig for HPV16 was consistent with p16 pathology reports (Fig. 5A; see also Table S1 in the supplemental material), with 80% of p16(+) tumors producing an AccSig value of more than 100. Of the eight p16(+) tumors with low or no HPV16 AccSig, four showed high signals for a subset of HPV16 probes or produced significant AccSig values for HPV26 or HPV92. The sliding window analysis recapitulated AccSig results and highlighted the differences between detection events for full or partial HPV16 genomes. In Fig. 5B, metagenome regions with a MAT score of more than 3,000 were compiled for each sample, and the individual probes within each region were ordered by map position in a plot of probe signals. This analysis detected a number of other organisms, including pathogenic oral bacteria, although the signals were lower than those of the HPV

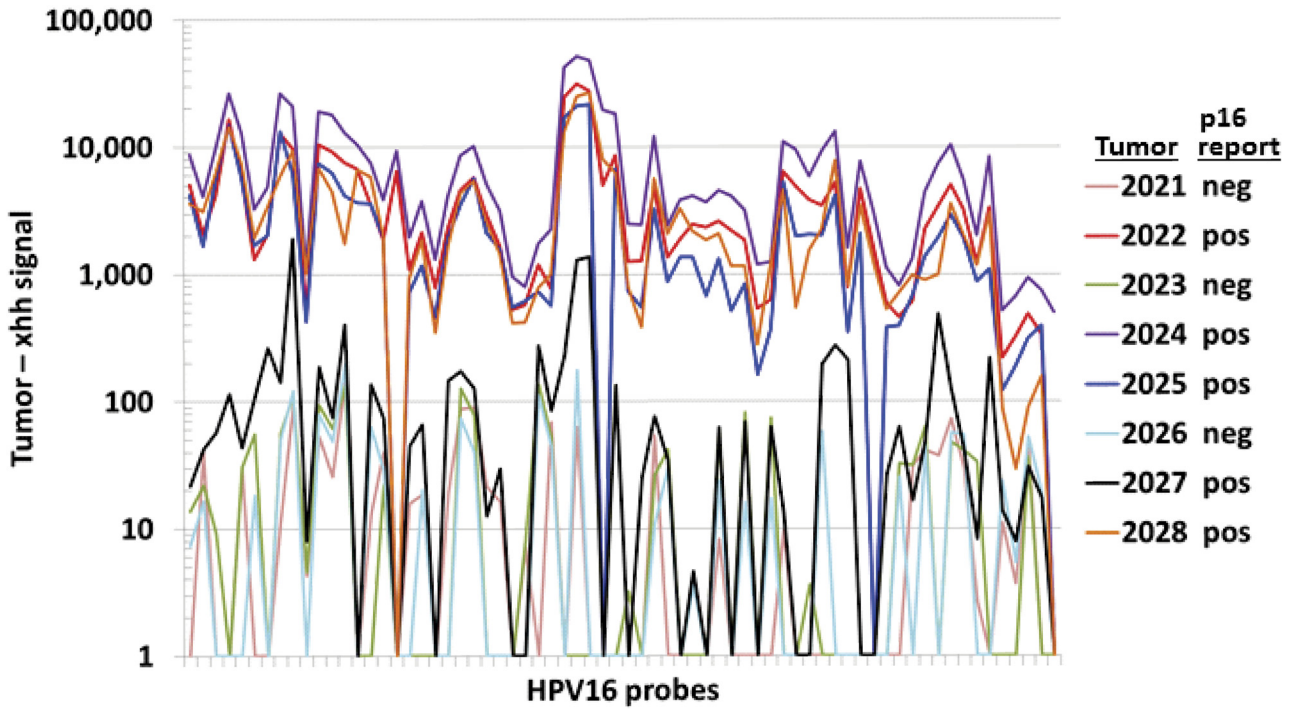

FIG 3 HPV16 detection in naturally infected tumor samples. Eight oral squamous cell carcinoma samples were assayed on PathoChips that include 68 probes for human papillomavirus 16 (HPV16). Clinical pathology results for p16 overexpression, a diagnostic marker correlated with oncogenic HPV infection, are indicated in the color key for each tumor's hybridization profile.

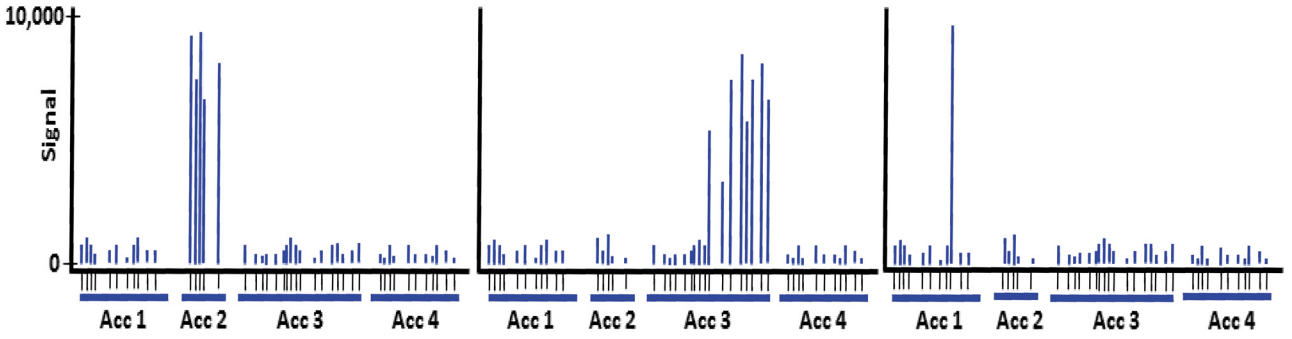

FIG 4 Model data illustrating three analysis strategies. Signals from individual probes (*x* axis) to four genome accessions (Acc) are plotted after hybridization to three hypothetical tumor samples. All probes for Acc2 show high signal in tumor 1 (left), so this candidate should be detectable by comparing the accession's all-probe averages from test samples with those of control samples. A subset of Acc3 probes show high signal in tumor 2 (middle), perhaps due to strain sequence differences or partial deletion of the genome, reducing the all-probe accession average and making detection more difficult. In this case, a sliding window analysis of local probe signals is not biased by accession annotation and may be more sensitive for candidate identification. A single probe for Acc1 has high signal in tumor 3 (right), so a third tier of analysis based solely on individual probe performance is needed to detect organisms not specifically targeted by the PathoChip but sharing sequence homology with one or a few probes.

genomes. These preliminary candidates will be investigated using confirmatory PCR and sequencing methods.

Analyses at the individual probe level also demonstrated utility for identifying candidates. A large majority of HPV16 probes passed a *t* test significance threshold for detection signals which were greater than background across the tumor population (Table 3), as would be expected for a genome that is so common in OSCC. Many HPV16 probes also passed the outlier test, indicating that although the signals are consistently different from background, the population's range of intensities is wide and therefore also contains outliers. In contrast, fewer HPV18 and HPV26 probes were significant by *t* test, reflecting the much lower apparent occurrence of these genomes in this tumor population (Table 3). However, the outlier analysis easily identified the relatively larger number of probes that produced HPV18 or HPV26 detections by AccSig or MAT score in a few positive samples. For these rarer candidates, some probes were significant by *t* test because they produced lower but consistent signals over background throughout the population, which may be an account of copy number of genomes present and is not surprising. This also illustrates the need to examine probe-level hybridization intensities, not just to analyze algorithm output scores, when considering candidates for follow-up validation, regardless of the method used for their initial identification.

Validation of PathoChip HPV16 detection. Inspection of HPV16 probe intensities after PathoChip screening (Fig. 6A) revealed patterns of high and low signal across the probe sets and tumor samples with high, low, or undetectable signal overall. PCR primers were designed to regions with high (f1 + r1) or moderate (f2 + r3) signals and adjacent to regions of low signal (primers r2 and r4) (Fig. 6A). PCR of genomic DNA from representative samples produced the appropriate amplicons from the high- and moderate-signal regions in tumors positive for HPV16 detection. Importantly, amplicons were not observed from HPV16-negative tumors (Fig. 6B). Occasional faint bands were observed for amplicons using the r2 or r4 primer as expected, as these had low signals in probe sets identified above.

Aliquots of the TransPlex products used for PathoChip screening were combined into six capture pools as indicated in Fig. 6A. The pools were mixed with a panel of biotinylated DNA probes that included HPV16 probes. Pooled DNA that hybridized to the probes was captured by magnetic streptavidin beads. Deep sequencing of libraries derived from the captured material produced a number of reads that map with high homology to the HPV16 genome (Fig. 6A), and these reads were enriched for the regions targeted by the capture probes but also included distal sequences. Mapping individual reads from each library showed that very few HPV16 templates were present in the sample pool containing only tumors that were HPV16 negative by PathoChip or p16 assays (pool 1, Fig. 6A and C). More HPV16 templates, up to 73 in pool 3, were observed in the libraries from HPV16-positive tumors. Interestingly, there were regions of high reads which showed high intensities in the majority of the tumors analyzed. The E4 region which was prevalent in the majority of the tumors (Fig. 6A to C) may provide a window into the transcription profiles of HPV16 in these particular type of OSCCs. The oncogenes E6 and E7 also showed a high number of signals in the tumors, but not as dramatic and surprising as the E4 open reading frame (ORF) region. However, this may be an interesting discovery which suggests a higher number of transcripts for the E4 ORFs in these tumors than was previously thought. Notably, the E1 region also showed greater signals in the tiled probes across the HPV16 genome. Predominantly, E4 seems to be the most prominent signal for the OSCC tumors and suggests a greater involvement of E4 in maintenance of the tumor by HPV than previously indicated.

DISCUSSION

The ability of a highly multiplexed, metagenomic assay to detect small nonhuman genomes in an overwhelming background of human sequences will be affected by several factors, including nucleic acid extraction and recovery, target size and copy number, participation in amplification reactions if used, and specific probe performance. The last three factors likely contributed to the differences in assay performance, in which 10,000 copies of JC or BK polyomavirus (5-kb genomes in a 4-kb double-stranded circular DNA plasmid vector) were detected with probe intensity ranges of 61 to 4,889 (JC virus, 42 probes) and 4 to 442 (BK virus, 9 probes). In contrast, adenovirus type 5 (36-kb genome, double-stranded linear nonintegrated DNA) was detected over an intensity range of

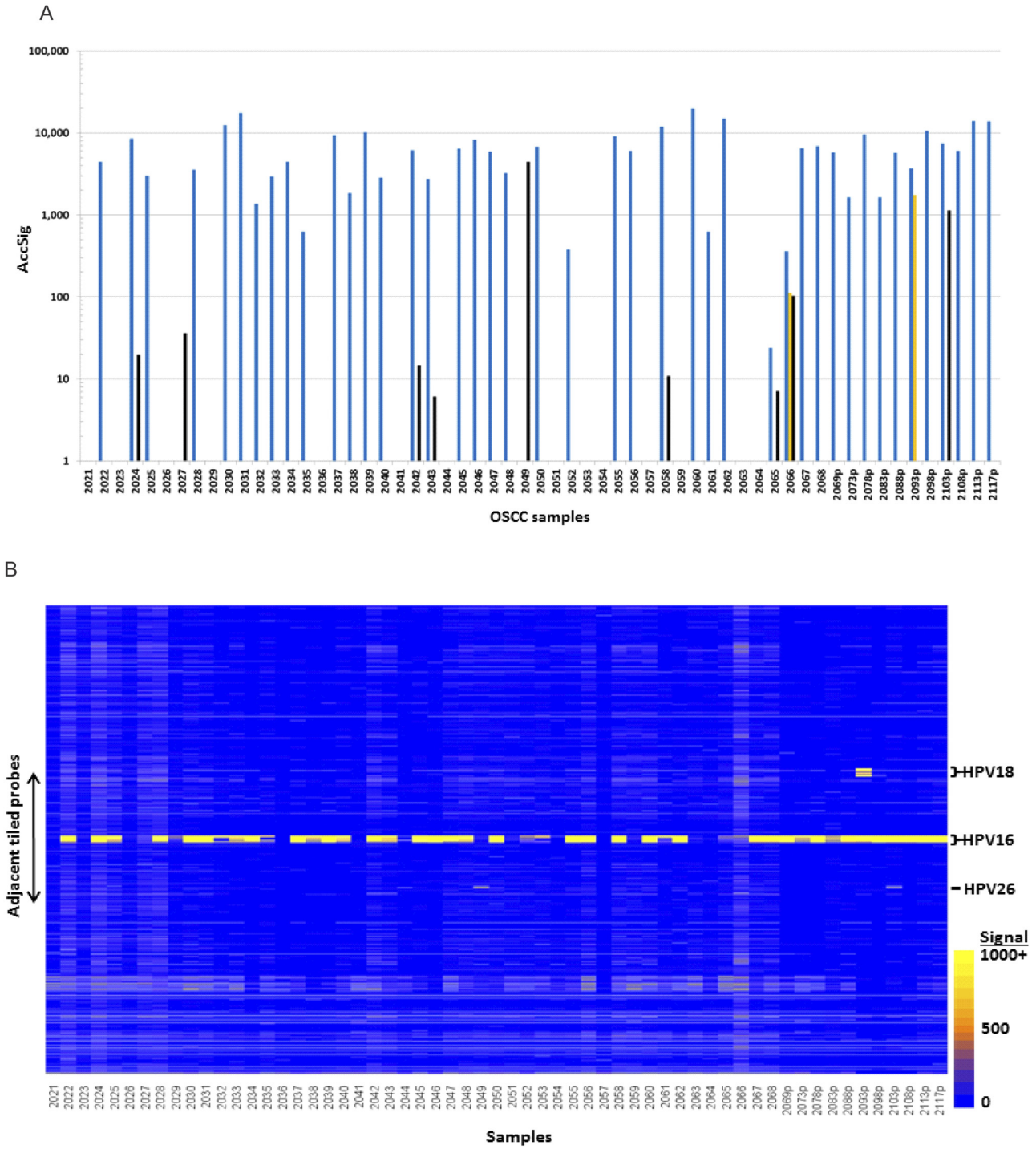

FIG 5 Accession average and sliding window analyses for HPV in tumors. (A) The accession signals (AccSig) for HPV16 (blue), HPV18 (orange), and HPV26 (black) were calculated from PathoChip results for 100 oral squamous cell carcinoma (OSCC) samples, assayed individually (2021 to 2068) or in pools (2069p to 2117p). (B) Signals (tumor minus xhh) for each probe in metagenome regions with high sliding window scores are shown as a heat map of probes (*y* axis rows) hybridized to the tumor samples in panel A.

342 to 65,325 using 63 probes and 100 target genome copies; differences in genome size and conformation may affect participation in whole-genome amplification reactions. Furthermore, probes clearly have different hybridization affinities despite sharing the same bioinformatic design criteria. PathoChip assay sensitivity will therefore vary across accessions and between protocol options, but the inclusion of multiple probes per accession and integration of candidates from different levels of data analysis provide avenues for optimizing the chances of detecting a pathogen in the screening projects. The HPV16 genome, for example, is a

TABLE 3 Individual probe analyses for human papillomavirus detection

Probe	No. of probes		
	HPV16	HPV18	HPV26
Total probes	68	85	13
Specific probes	67	84	11
Pass *t* test	64	11	4
Pass outlier test	65	66	9
Conserved probes	1	1	2
Pass *t* test	1	1	0
Pass outlier test	1	0	2

7.9-kb double-stranded DNA (dsDNA) circle and was detected by 67 of 68 probes with intensities ranging from 217 to 31,475 in a naturally infected tissue specimen (OSCC no. 2022).

Integrating multiple probe analyses which include accession-level, sliding window, and individual probe comparisons detected HPV16 in 34 of 48 OSCC tumors individually tested by PathoChip screening, a 71% occurrence rate somewhat higher than the estimated 63% rate previously reported (29, 30) but not unreasonable given the rapidly increasing prevalence of papillomaviruses in oropharyngeal cancers (31). The results of the assay were highly concordant with the molecular pathology reports for p16 overexpression and in some cases suggested that an HPV strain other than HPV16 may be responsible. HPV16 detections by PathoChip assays were confirmed by PCR using primers that are independent of PathoChip probes and by recovery and sequencing of HPV16 regions located outside those targeted by capture probes on the HPV genome.

The ability of the PathoChIP to combine saturation probe sets and RNA and DNA detection enhances the screening for known oncogenic pathogens. If sufficient target copies are present in a sample, inferences regarding genomic structural variation and RNA expression levels may be possible. For HPV16, probes mapping to early gene transcripts produced more overall signal than those for late genes in OSCC samples; this is consistent with studies of actively infected cells and the oncogenic effects of E6/E7 expression (32, 33). Moreover, the transcription of HPV at the level of detail that we are probing here is greater than previously investigated and suggests a potential role for other transcripts, including the E4 ORF and related antigen, in maintenance of the transformed state in the tumors. Signals from probes to late gene sequences were similar to or somewhat higher than those of probes to intergenic HPV16 sequences. Therefore, the boost in early gene signals is likely due to the RNA portion of the sample target preparation. Among the early genes, strong signals were observed for E6/E7 sequences, and for the E4 region of E2, which is known to be a highly abundant RNA splicing product from the primary transcript (34). Detailed interpretation of these data is complicated by the ability of HPV16 to exist in episomal and multiple host-genome integrated forms (35), but probe signal differences within and between tumors will provide the identification of potential agents having oncogenic activities and so lead to new lines of investigation as a follow-up to the initial screening experiment.

Averaging probe signals by accession provided a rapid and rather uncomplicated means to summarize the data and collect the strongest detection candidates. The sliding window analysis generally matched AccSig results but provided better ability to distinguish variants within the set of samples and offers the potential to detect candidates represented by only a portion of an accession. As used here, the MAT algorithm did require more labor because it was applied to each sample in separate operations, but this could be addressed by future automated scripting. Analyses at the individual probe level helped to explain how candidates arose in the AccSig and MAT results and are likely the only way in which previously unknown pathogens with some sequence homology to a conserved (or specific) probe can be detected. Thus, a PathoChip screening project can generate a list of candidates prioritized by the magnitude of detection, detection via multiple analysis strategies, and the rate of detection across the sample population. Combining these results with annotations for the virus or pathogenic microorganism such as host range, tissue specificity, or prevalence in the general population will assist in determination of which agents deserve further attention. This approach is likely to provide a signature of a particular cancer or disease with agents with various degrees of contribution. A window into the natural conditions for commensal and pathogenic organisms will greatly enhance our ability to diagnose and treat cancer and other possible diseases not yet linked to specific agents.

The PathoChip screening assay described here supported faster laboratory and data analysis turnarounds than those for deep sequencing of whole-genome tumor DNA or RNA and coverage of viral and eukaryotic genomes not assayed by 16S rRNA approaches. The Agilent SurePrint platform is relatively economical compared to other microarray formats and is flexible for quick production of customized probe subsets or updated metagenome compilations, as well as being compatible with a variety of upstream sample preparation strategies. The PathoChip metagenomic assay allows for a comprehensive assessment of the frequency of coinfection by multiple organisms and their correlation with driving oncogenic events. These events can lead to proliferation early in the infection process as well as over an extensive period during which the contributions by these agents may vary or have specific effects on the host cell important for disease development. The data analysis workflows will test for statistically significant interactions between these infectious agents. Critically, as these studies unfold, the PathoChip data in combination with patient genotyping, RNA profiling, and clinical data may be used to search for genetic or environmental predispositions that influence the host-pathogen interactions important for initiation and maintenance of the cancer phenotype.

MATERIALS AND METHODS

Microarray design. National Center for Biotechnology Information (NCBI) databases for genome, gene, and nucleotide accessions were queried (http://www.ncbi.nlm.nih.gov/pubmed) for all taxonomy virus annotations and for accessions from prokaryotic and eukaryotic human pathogen lists compiled by literature searches and web resources (http://www.niaid.nih.gov: Emerging and Re-emerging Infectious Diseases, Category A, B, and C Priority Pathogens). The resulting accessions were assembled into a nonredundant concatenation with 100-N nucleotide separators between accessions. This metagenome was divided into 58 "chromosomes" each around 5 to 10 million nucleotides (nt) in length and submitted to Agilent Technologies (Santa Clara, CA) as a custom design project. Probe sequences, at a maximum of 60 nt with nonhybridizing spacers, were selected using the Agilent array comparative genomic hybridization (aCGH) design algorithms and then filtered for low likelihood of cross-hybridization to human genomic sequences.

Independently, low-complexity regions in the metagenome were

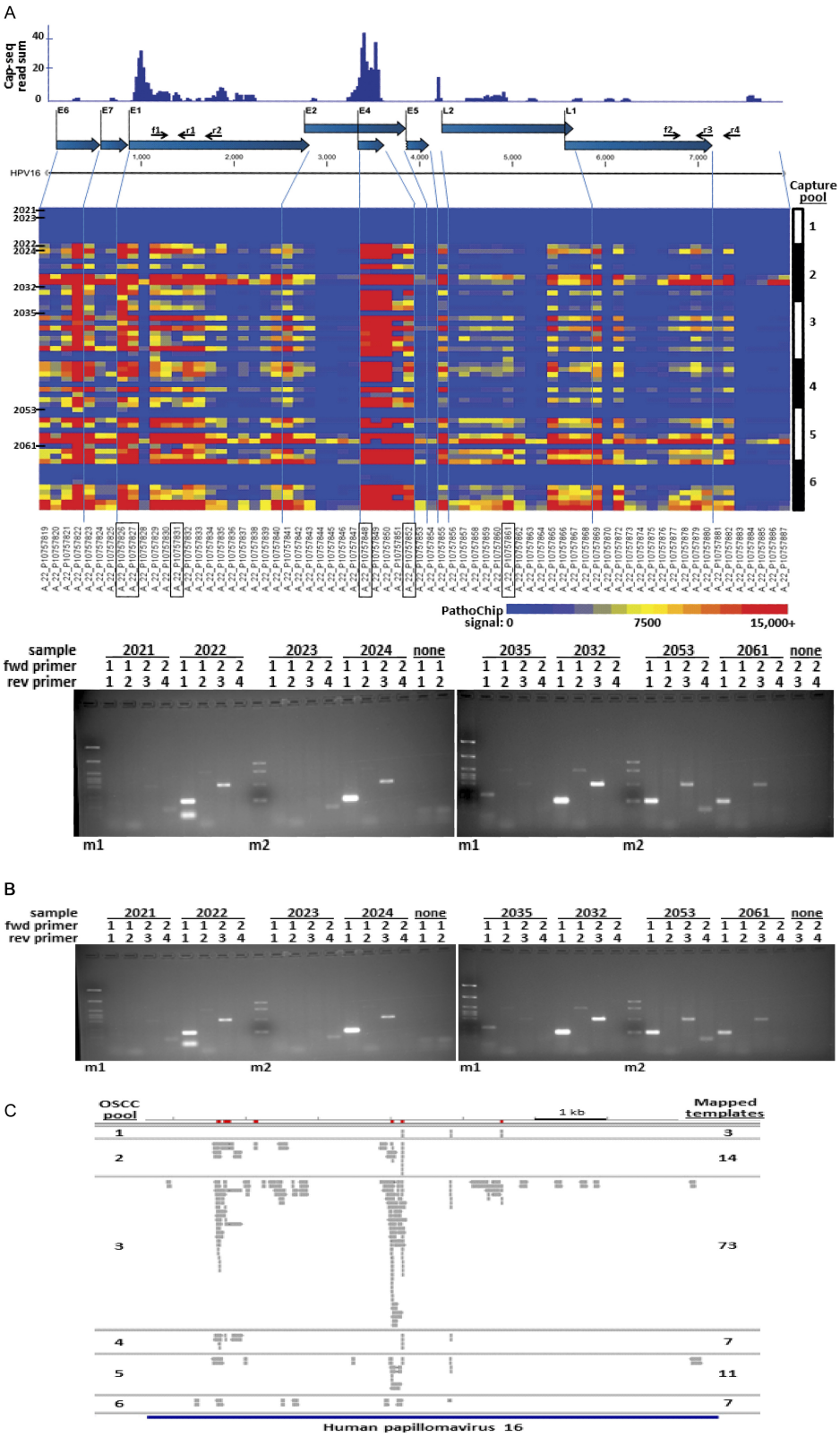

FIG 6 Confirmation of HPV16 detection. (A) The heat map indicates test minus xhh signals for every HPV16 probe (columns) from PathoChip assays of the OSCC samples (rows). Row numbers are indicated for samples that are examples of no HPV16 signal (2021 and 2023), hybridization to nearly all probes (2022 and 2024), or hybridization to a smaller subset of probes (2032, 2035, 2053, and 2061). Probe locations are indicated relative to the transcript map for early (E) and late (L) genes, and black arrows show the positions of forward (f) and reverse (r) PCR primers. Probe names in boxes correspond to the oligomers used for capture bead enrichment and deep sequencing (cap-seq) of samples that were pooled as marked by the right axis bars. The histogram shows the sum of cap-seq

(Continued)

masked using mdust (http://doc.bioperl.org/bioperl-run/lib/Bio/Tools/Run/Mdust.html) followed by BLASTN 2.0MP-WashU (Advanced Biocomputing, LLC, St. Louis, MO) identification of unique regions in viral accessions (36). Criteria for unique regions were 250 to 300 bp and <50 contiguous bp with >70% identity to a sequence in any other metagenome accession. Conserved viral regions were similarly identified using criteria of 70 to 300 bp and >70% identity to at least one other virus but not to human sequences.

Agilent-designed probes that mapped to unique or conserved regions of the pathogen genomes, or any prokaryotic or eukaryotic pathogen accession, were added to the microarray design by default if fewer than 10 probes were available for the source accession. Otherwise, the probes were filtered for minimum interprobe spacing of 100 bp and distribution that roughly covers the full length of each accession while limiting the number of probes to 10 to 20 per accession. The number of probes was not restricted for known oncogenic viral agents, creating a saturation tiling set covering these accessions. Entire genome sequences were covered to the extent possible with all available Agilent-designed probes. The microarray was supplemented with an additional number of predesigned aCGH probes for 660 genes and 602 intergenic regions from the human genome and *Saccharomyces cerevisiae*. Probes and accession annotations are available in the Gene Expression Omnibus (http://www.ncbi.nlm.nih.gov/geo/).

Sample preparation. Purified phiX174 virion DNA was purchased from New England Biolabs (N3023S; Ipswich, MA, USA), total DNA from human MRC-5 cells infected with cytomegalovirus (human herpesvirus 5 strain AD169) was ATCC VR-538D, total DNA from human A549 cells infected with adenovirus type 5 (HAdV-5 strain Adenoid 75) was ATCC VR-5D, and total RNA from human HEp-2 cells infected with respiratory syncytial virus (HRSV strain Long) was ATCC VR-26D, all purchased from ATCC (Manassas, VA, USA). Plasmid minipreps were prepared from pBR322 subclones carrying JC or BK polyomavirus genomes (J. C. Alwine, University of Pennsylvania, Philadelphia, PA) and from pUC19 carrying the human papillomavirus 16 (HPV16) genome (obtained from Peter Howley, Harvard Medical School, Boston, MA).

Oropharyngeal squamous cell carcinoma tumor samples were obtained from the Abramson Cancer Center's Tumor Tissue and Biospecimen Bank (https://somapps.med.upenn.edu/pbr/portal/tumor/). All samples were reviewed by our resident pathologist for case history and confirmed for tumor type and demarcation of the cancer cells. If significant adjacent normal tissue was present, sections were mounted on noncharged glass slides for dissection of tumor tissue using a template slide with a hematoxylin-and-eosin (H&E)-stained section with the cancer region clearly demarcated. Specimens containing mostly cancer cells were provided as paraffin rolls. The rolls or mounted sections (minimum of 5; 10 μm each) from formalin-fixed, paraffin-embedded (FFPE) tumors were used for sequential DNA and RNA extraction using the AllPrep DNA/RNA FFPE kit (Qiagen, Germantown, MD, USA). Nucleic acid quality control assessments included $A_{260/280}$ ratios, yield, and size distribution by agarose gel electrophoresis in 0.5× Tris-borate EDTA buffering system. As expected, formalin-exposed RNA was partially degraded. However, recovery of most samples was relatively good, allowing for further processing. In most of the samples, the fragment sizes were acceptable and were moved ahead for cDNA conversion.

Whole-genome amplifications (WGAs) of genomic DNA and/or cDNA from random-primed, reverse-transcribed total RNA were performed with the Illustra GenomiPhi v2 kit (GE Healthcare Bio-Sciences, Pittsburgh, PA, USA), the Ovation WGA system (NuGEN, San Carlos, CA, USA), and GenomePlex or TransPlex kits (WGA2 and WTA2; Sigma-Aldrich, St. Louis, MO) using manufacturer-recommended protocols and input amounts. Amplification products were purified with the QIAquick PCR purification kit (Qiagen), and 2 μg was used for Cy3 dye labeling by the SureTag labeling kit (Agilent). Cy5 dye labeling was performed on 2 μg of human reference DNA from the Agilent SureTag kit, without prior WGA (experiment 1, Table 1) or after WGA (other experiments), as a control to report probe cross-hybridization to human DNA. Labeled DNA was purified with SureTag kit spin columns, and specific activities were calculated for use in hybridization reactions.

Microarray production and processing. SurePrint glass slide microarrays (Agilent Technologies Inc.) were manufactured with 60-nt DNA oligomers synthesized in 60,000 features on eight replicate arrays per slide. PathoChip v2a and v2b contained 60,000 probes to unique target regions and conserved plus saturation target regions, respectively. PathoChip v3 contained 37,704 probes to unique targets and 23,627 probes to conserved targets or to saturate known oncogenic and pathogenic viral agents.

Labeled samples were hybridized to microarrays as described in the Agilent Oligonucleotide Array-Based CGH for Genomic DNA Analysis protocol (version 7.2, G4410-90010). Master mixes containing aCGH blocking agent, HI-RPM hybridization buffer, and Cot-1 DNA (pilot assays only) were added to a mixture of the entire labeled test sample and the xhh DNA control sample, denatured, and hybridized to arrays under 8-chamber gasket slides at 65°C with 20-rpm rotation for 40 h in an Agilent hybridization oven. Arrays were processed using wash procedure A and scanned on an Agilent SureScan G4900DA microarray scanner.

Microarray data analysis. Scanned microarray images were analyzed using Agilent Feature Extraction software to calculate average pixel intensity and subtract local background for each feature. Images were manually examined to note any arrays affected by high background, scratches, or other technical artifacts. The intensity distribution and channel balance were not used for quality control because they are expected to have little or no signal, except for the control human probes.

Feature intensities for Cy3 and Cy5 channels were imported into the Partek Genomics Suite (Partek Inc., St. Louis, MO, USA). The average intensity for human intergenic control probes was calculated for cohybridized test and xhh DNA samples, and a scale factor was determined which would make the Cy5 xhh DNA average equal to the Cy3 average. The Cy5 intensities for all PathoChip probes were then multiplied by the scale factor to normalize for differences in dye performance. Cy3/Cy5 ratios and Cy3-Cy5 subtractions were calculated for each probe to provide input for dual-channel or single-channel analysis pipelines, respectively. Accession average (AccAvg) was defined as the average Cy3 or Cy5 intensity across all probes for one accession, and accession signal (AccSig) was defined as AccAvg(Cy3) − AccAvg(Cy5).

Model-based analysis of tiling arrays (MAT) (28) as implemented in Partek was used for sliding window analysis of probe signals (Cy3 minus Cy5) for each tumor sample. MAT parameters were *P* value cutoff of 0.99, window of 5,000 bp, minimum number of positive probes of 5, and dis-

Figure Legend Continued

reads that mapped to the HPV16 genome from all sample pools; the *x* axis shows map coordinates scaled to match the transcript map. (B) PCR using the forward (fwd) and reverse (rev) primers shown in panel a detected at least one HPV16 region in samples with hybridization to most or some PathoChip HPV16 probes and no detection in samples that were negative for PathoChip signal or were no-template controls. The m1 marker is phiX174 HaeIII digest, and the m2 marker contains the four amplicons produced from a plasmid carrying the HPV16 genome. (C) The individual reads obtained from cap-seq are shown for the sample pools from panel A. Pool 1 contained seven samples with low or no hybridization signal to HPV16 probes in PathoChip screening assays; 71% of the remaining samples were positive for PathoChip HPV16 detection. Whole-genome amplified DNA plus cDNA was hybridized to a set of six biotinylated HPV16 probes, captured on streptavidin beads, and used for tagmentation library preparation and deep sequencing with paired-end 250-nt reads. (Tagmentation is the process of tagging the fragmented DNA generated during library perpetration.) Reads (gray arrows) that map to the HPV16 reference genome sequence (blue) cluster around the capture probe locations (red segments in the 1-kb coordinate map), but templates up to 3 kb away from a capture probe were also recovered.

card value of 0%. Candidate regions were classified by MAT scores of 30 to 300, 300 to 3,000, and >3,000.

Partek analysis of variance (ANOVA) tools were used to perform paired *t* tests with multiple testing correction using all tumor samples as replicates of the test condition and cohybridized xhh DNA replicates as the control condition. Comparisons were performed at the accession level using AccAvg(Cy3) versus AccAvg(Cy5), and at the individual probe level using Cy3 versus Cy5 intensity values. Significance thresholds were set at a step-up false discovery rate of <0.05 and fold difference of >2. An outlier analysis was also performed at accession and probe levels by calculating the standard deviation of AccSig or probe signal across all tumors and filtering for any values that were 2 or more standard deviations higher than the population mean.

HPV16 PCR and capture sequencing. PCR amplification reaction mixtures for HPV16 detection contained 100 ng of tumor DNA and primer f1 (5′ AAGCGAAGACAGCGGGTATG), f2 (5′ AGGAGTACCTA CGACATGGGG), r1 (5′ TGGTGTTTGGCATATAGTGTGTC), r2 (5′ TGGCGTGTCTCCATACACTT), r3 (5′ GTGGTGGGTGTAGCTTTTC GT), or r4 (5′ TGGCAAGCAGGAAACGTACA). DNA was denatured at 94°C for 2 min, followed by 30 cycles of 94°C for 30 s, 57°C for 60 s, and 65°C for 60 s.

Magnetic bead capture was used to create libraries of targeted sequences for deep sequencing. Selected PathoChip probes with high signals for candidate organisms were synthesized as 5′-biotinylated DNA oligomers (Integrated DNA Technologies, Coralville, IA, USA), mixed as a 36-probe panel, including six probes for HPV16 (Fig. 6A), and hybridized to pools of tumor targets. Targets were captured by pooling the TransPlex products used for PathoChip screening (100 tumors over six pools) and then adding a probe panel aliquot containing 2.5 pmol of each probe to 150 ng of each target pool in 100-μl reaction mixtures with 1× TMAC buffer (3 M tetramethylammonium chloride, 0.1% Sarkosyl, 50 mM Tris-HCl, 4 mM EDTA, pH 8.0). The reaction mixtures were denatured at 100°C for 10 min followed by hybridization at 60°C for 3 h. M-280 streptavidin Dynabeads (Life Technologies, Carlsbad, CA, USA) (1,530 μg) were then added with continuous mixing at room temperature for 3 h, followed by three washes of the magnetically captured bead-probe-target complexes with 1 ml 2× SSC (1× SSC is 0.15 M NaCl plus 0.015 M sodium citrate) and three washes with 1 ml 0.1× SSC. Captured single-stranded target DNA was eluted in 50 μl Tris-EDTA (TE) at 100°C for 10 min.

The six capture eluates (1 μl) were reamplified by GenomePlex reactions (WGA3; Sigma-Aldrich), purified by Agencourt AMPure XP beads (Beckman Coulter, Indianapolis, IN, USA) using the manufacturer's protocol, and assessed for yield by Qubit double-stranded DNA (dsDNA) assays (Life Technologies, Inc.) and for size distribution by agarose gel electrophoresis. Sequencing libraries were prepared using the Nextera XT DNA sample preparation kit (Illumina, San Diego, CA, USA), with dual indexing and bead library normalization according to the manufacturer's protocols. After Qubit quantitation, libraries were submitted to the Washington University Genome Technology Access Center (St. Louis, MO) for quantitative PCR (qPCR) quality control measurements, library pooling, and sequencing on one flow cell of an Illumina MiSeq instrument with paired-end 250-nt reads. Approximately 400,000 reads from the six OSCC libraries generated were aligned to the PathoChip metagenome or the human genome using the Bowtie2 aligner (36) in sensitive-local mode. Reads mapping to HPV16 with MapQ scores of 20 or better were identified using Integrative Genomics Viewer 2.3.25 (37).

Institutional oversight. The research described does not involve animals. Tumors from human subjects were collected with informed consent for research use and were received as deidentified samples. This study was approved by the University of Pennsylvania institutional review board.

SUPPLEMENTAL MATERIAL

Supplemental material for this article may be found at http://mbio.asm.org/lookup/suppl/doi:10.1128/mBio.01714-14/-/DCSupplemental.

Table S1, DOCX file, 0.1 MB.

ACKNOWLEDGMENTS

We greatly appreciate the expertise and advice contributed by Brian Brunk, John Tobias, Christopher P. Sarnowski, Fang Chen, R. Ben Isett, and Natalie Shih (University of Pennsylvania) and Michelle Filipek, Barbara Teets, and Josh Wang (Agilent Technologies Inc.).

This project was funded by grants to E.S.R. from the Abramson Cancer Center of the University of Pennsylvania, Agilent Technologies Inc., and the Avon Foundation.

The authors have no sources of financial support that pose a conflict of interest for conducting or interpreting the work presented in this paper.

REFERENCES

1. **de Martel C, Ferlay J, Franceschi S, Vignat J, Bray F, Forman D, Plummer M.** 2012. Global burden of cancers attributable to infections in 2008: a review and synthetic analysis. Lancet Oncol. **13:**607–615. http://dx.doi.org/10.1016/S1470-2045(12)70137-7.
2. **Relman DA.** 2012. Microbiology: learning about who we are. Nature **486:**194–195. http://dx.doi.org/10.1038/486194a.
3. **The Human Microbiome Project Consortium.** 2012. Structure, function and diversity of the healthy human microbiome. Nature **486:**207–214. http://dx.doi.org/10.1038/nature11234.
4. **Laass MW, Roggenbuck D, Conrad K.** 2014. Diagnosis and classification of Crohn's disease. Autoimmun. Rev. **13:**467–471. http://dx.doi.org/10.1016/j.autrev.2014.01.029.
5. **Major G, Spiller R.** 2014. Irritable bowel syndrome, inflammatory bowel disease and the microbiome. Curr. Opin. Endocrinol. Diabetes Obes. **21:**15–21. http://dx.doi.org/10.1097/MED.0000000000000032.
6. **Schwarzberg K, Le R, Bharti B, Lindsay S, Casaburi G, Salvatore F, Saber MH, Alonaizan F, Slots J, Gottlieb RA, Caporaso JG, Kelley ST.** 2014. The personal human oral microbiome obscures the effects of treatment on periodontal disease. PLoS One **9:**e86708. http://dx.doi.org/10.1371/journal.pone.0086708.
7. **Scharschmidt TC, Fischbach MA.** 2013. What lives on our skin: ecology, genomics and therapeutic opportunities of the skin microbiome. Drug Discov. Today Dis. Mech. **10:**3–4. http://dx.doi.org/10.1016/j.ddtec.2012.10.014.
8. **Martinez FJ, Erb-Downward JR, Huffnagle GB.** 2013. Significance of the microbiome in chronic obstructive pulmonary disease. Ann. Am. Thorac. Soc. **10**(Suppl):S170–S179. http://dx.doi.org/10.1513/AnnalsATS.201306-204AW.
9. **Segal LN, Rom WN, Weiden MD.** 2014. Lung microbiome for clinicians. New discoveries about bugs in healthy and diseased lungs. Ann. Am. Thorac. Soc. **11:**108–116. http://dx.doi.org/10.1513/AnnalsATS.201310-339FR.
10. **Sze M, Dimitriu PA, Suzuki M, McDonough JE, Gosselink JV, Elliott MW, Mohn WW, Hayashi S, Hogg JC.** 2014. Host response to the lung microbiome in lung tissue undergoing emphysematous destruction. Ann. Am. Thorac. Soc. **11**(Suppl 1):S77. http://dx.doi.org/10.1513/AnnalsATS.201306-198MG.
11. **Gjymishka A, Coman RM, Brusko TM, Glover SC.** 2013. Influence of host immunoregulatory genes, ER stress and gut microbiota on the shared pathogenesis of inflammatory bowel disease and type 1 diabetes. Immunotherapy **5:**1357–1366. http://dx.doi.org/10.2217/imt.13.130.
12. **Kamada N, Núñez G.** 2014. Regulation of the immune system by the resident intestinal bacteria. Gastroenterology **146:**1477–1488. http://dx.doi.org/10.1053/j.gastro.2014.01.060.
13. **Koboziev I, Reinoso Webb C, Furr KL, Grisham MB.** 2014. Role of the enteric microbiota in intestinal homeostasis and inflammation. Free Radic. Biol. Med. **68C:**122–133. http://dx.doi.org/10.1016/j.freeradbiomed.2013.11.008.
14. **Ooi JH, Waddell A, Lin YD, Albert I, Rust LT, Holden V, Cantorna MT.** 2014. Dominant effects of the diet on the microbiome and the local and systemic immune response in mice. PLoS One **9:**e86366. http://dx.doi.org/10.1371/journal.pone.0086366.
15. **Iida N, Dzutsev A, Stewart CA, Smith L, Bouladoux N, Weingarten RA, Molina DA, Salcedo R, Back T, Cramer S, Dai RM, Kiu H, Cardone M, Naik S, Patri AK, Wang E, Marincola FM, Frank KM, Belkaid Y, Trinchieri G, Goldszmid RS.** 2013. Commensal bacteria control cancer response to therapy by modulating the tumor microenvironment. Science **342:**967–970. http://dx.doi.org/10.1126/science.1240527.
16. **Xuan C, Shamonki JM, Chung A, DiNome ML, Chung M, Seiling PA,**

Lee DJ. 2014. Microbial dysbiosis is associated with human breast cancer. PLoS One **9:**e83744. http://dx.doi.org/10.1371/journal.pone.0083744.
17. **Cox MJ, Cookson WO, Moffatt MF.** 2013. Sequencing the human microbiome in health and disease. Hum. Mol. Genet. **22:**R88–R94. http://dx.doi.org/10.1093/hmg/ddt398.
18. **Ma Y, Madupu R, Karaoz U, Nossa CW, Yang L, Yooseph S, Yachimski PS, Brodie EL, Nelson KE, Pei Z.** 2014. Human papillomavirus community in healthy persons, defined by metagenomics analysis of HMP (human microbiome project) shotgun sequencing datasets. J. Virol. **88:**4786–4797. http://dx.doi.org/10.1128/JVI.00093-14.
19. **Brodie EL, Desantis TZ, Joyner DC, Baek SM, Larsen JT, Andersen GL, Hazen TC, Richardson PM, Herman DJ, Tokunaga TK, Wan JM, Firestone MK.** 2006. Application of a high-density oligonucleotide microarray approach to study bacterial population dynamics during uranium reduction and reoxidation. Appl. Environ. Microbiol. **72:**6288–6298. http://dx.doi.org/10.1128/AEM.00246-06.
20. **Chen EC, Miller SA, DeRisi JL, Chiu CY.** 2011. Using a pan-viral microarray assay (Virochip) to screen clinical samples for viral pathogens. J. Vis. Exp. **50:**2536. http://dx.doi.org/10.3791/2536.
21. **Tu Q, Yu H, He Z, Deng Y, Wu L, Van Nostard JD, Zhou A, Voordeckers J, Qin Y, Hemme CL, Shi Z, Xue K, Yaun T, Wang A, Zhou J.** 2014. GeoChip 4: a functional gene array-based high throughput environmental technology for microbial community analysis. Mol. Ecol. Resour. **14:**914–928. http://dx.doi.org/10.1111/1755-0998.12239.
22. **Wong CW, Heng CL, Wan Yee L, Soh SW, Kartasasmita CB, Simoes EA, Hibberd ML, Sung WK, Miller LD.** 2007. Optimization and clinical validation of a pathogen detection microarray. Genome Biol. **8:**R93. http://dx.doi.org/10.1186/gb-2007-8-5-r93.
23. **Norman JM, Handley SA, Virgin HW.** 2014. Kingdom-agnostic metagenomics and the importance of complete characterization of enteric microbial communities. Gastroenterology **146:**1459–1469. http://dx.doi.org/10.1053/j.gastro.2014.02.001.
24. **Sato M, Ohtsuka M, Ohmi Y.** 2005. Usefulness of repeated GenomiPhi, a phi29 DNA polymerase-based rolling circle amplification kit, for generation of large amounts of plasmid DNA. Biomol. Eng. **22:**129–132. http://dx.doi.org/10.1016/j.bioeng.2005.05.001.
25. **Arneson N, Hughes S, Houlston R, Done S.** 2008. GenomePlex whole-genome amplification. CSH Protoc. 2008:4920. http://dx.doi.org/10.1101/pdb.prot4920.
26. **Hirsch D, Camps J, Varma S, Kemmerling R, Stapleton M, Ried T, Gaiser T.** 2012. A new whole genome amplification method for studying clonal evolution patterns in malignant colorectal polyps. Genes Chromosomes Cancer **51:**490–500. http://dx.doi.org/10.1002/gcc.21937.
27. **Robinson M, Schache A, Sloan P, Thavaraj S.** 2012. HPV specific testing: a requirement for oropharyngeal squamous cell carcinoma patients. Head Neck Pathol. **6:**S83–S90. http://dx.doi.org/10.1007/s12105-012-0370-7.
28. **Johnson WE, Li W, Meyer CA, Gottardo R, Carroll JS, Brown M, Liu XS.** 2006. Model-based analysis of tiling-arrays for ChIP-chip. Proc. Natl. Acad. Sci. U. S. A. **103:**12457–12462. http://dx.doi.org/10.1073/pnas.0601180103.
29. **Gillison ML, Chaturvedi AK, Lowy DR.** 2008. HPV prophylactic vaccines and the potential prevention of noncervical cancers in both men and women. Cancer **113**(10 Suppl):3036–3046. http://dx.doi.org/10.1002/cncr.23764.
30. **Wu X, Watson M, Wilson R, Saraiya M, Cleveland JL, Markowitz L.** 2012. Human papillomavirus-associated cancers—United States, 2004-2008. MMWR Morb. Mortal. Wkly. Rep. **61:**258–261.
31. **Chaturvedi AK, Engels EA, Pfeiffer RM, Hernandez BY, Xiao W, Kim E, Jiang B, Goodman MT, Sibug-Saber M, Cozen W, Liu L, Lynch CF, Wentzensen N, Jordan RC, Altekruse S, Anderson WF, Rosenberg PS, Gillison ML.** 2011. Human papillomavirus and rising oropharyngeal cancer incidence in the United States. J. Clin. Oncol. **29:**4294–4301. http://dx.doi.org/10.1200/JCO.2011.36.4596.
32. **Cumming SA, Cheun-Im T, Milligan SG, Graham SV.** 2008. Human papillomavirus type 16 late gene expression is regulated by cellular RNA processing factors in response to epithelial differentiation. Biochem. Soc. Trans. **36:**522–524. http://dx.doi.org/10.1042/BST0360522.
33. **Thierry F.** 2009. Transcriptional regulation of the papillomavirus oncogenes by cellular and viral transcription factors in cervical carcinoma. Virology **384:**375–379. http://dx.doi.org/10.1016/j.virol.2008.11.014.
34. **Doorbar J.** 2013. The E4 protein; structure, function and patterns of expression. Virology **445:**80–98. http://dx.doi.org/10.1016/j.virol.2013.07.008.
35. **Xu B, Chotewutmontri S, Wolf S, Klos U, Schmitz M, Dürst M, Schwarz E.** 2013. Multiplex identification of human papillomavirus 16 DNA integration sites in cervical carcinomas. PLoS One **8:**e66693. http://dx.doi.org/10.1371/journal.pone.0066693.
36. **Langmead B, Trapnell C, Pop M, Salzberg SL.** 2009. Ultrafast and memory-efficient alignment of short DNA sequences to the human genome. Genome Biol. **10:**R25. http://dx.doi.org/10.1186/gb-2009-10-3-r25.
37. **Thorvaldsdóttir H, Robinson JT, Mesirov JP.** 2013. Integrative Genomics Viewer (IGV): high-performance genomics data visualization and exploration. Brief. Bioinform. **14:**178–192. http://dx.doi.org/10.1093/bib/bbs017.
38. **Wang D, Coscoy L, Zylberberg M, Avila PC, Boushey HA, Ganem D, DeRisi JL.** 2002. Microarray-based detection and genotyping of viral pathogens. Proc. Natl. Acad. Sci. U. S. A. **99:**15687–15692. http://dx.doi.org/10.1073/pnas.242579699.
39. **Chiu CY, Rouskin S, Koshy A, Urisman A, Fischer K, Yagi S, Schnurr D, Eckburg PB, Tompkins LS, Blackburn BG, Merker JD, Patterson BK, Ganem D, DeRisi JL.** 2006. Microarray detection of human parainfluenzavirus 4 infection associated with respiratory failure in an immunocompetent adult. Clin. Infect. Dis. **43:**e71–e76. http://dx.doi.org/10.1086/507896.
40. **Urisman A, Molinaro RJ, Fischer N, Plummer SJ, Casey G, Klein EA, Malathi K, Magi-Galluzzi C, Tubbs RR, Ganem D, Silverman RH, DeRisi JL.** 2006. Identification of a novel gammaretrovirus in prostate tumors of patients homozygous for R462Q RNASEL variant. PLoS Pathog. **2:**e25. http://dx.doi.org/10.1371/journal.ppat.0020025.
41. **Chiu CY, Alizadeh AA, Rouskin S, Merker JD, Yeh E, Yagi S, Schnurr D, Patterson BK, Ganem D, DeRisi JL.** 2007. Diagnosis of a critical respiratory illness caused by human metapneumovirus by use of a pan-virus microarray. J. Clin. Microbiol. **45:**2340–2343. http://dx.doi.org/10.1128/JCM.00364-07.
42. **Kistler A, Avila PC, Rouskin S, Wang D, Ward T, Yagi S, Schnurr D, Ganem D, DeRisi JL, Boushey HA.** 2007. Pan-viral screening of respiratory tract infections in adults with and without asthma reveals unexpected human coronavirus and human rhinovirus diversity. J. Infect. Dis. **196:**817–825. http://dx.doi.org/10.1086/520816.
43. **Chiu CY, Greninger AL, Kanada K, Kwok T, Fischer KF, Runckel C, Louie JK, Glaser CA, Yagi S, Schnurr DP, Haggerty TD, Parsonnet J, Ganem D, DeRisi JL.** 2008. Identification of cardioviruses related to Theiler's murine encephalomyelitis virus in human infections. Proc. Natl. Acad. Sci. U. S. A. **105:**14124–14129. http://dx.doi.org/10.1073/pnas.0805968105.
44. **Kistler AL, Gancz A, Clubb S, Skewes-Cox P, Fischer K, Sorber K, Chiu CY, Lublin A, Mechani S, Farnoushi Y, Greninger A, Wen CC, Karlene SB, Ganem D, DeRisi JL.** 2008. Recovery of divergent avian bornaviruses from cases of proventricular dilatation disease: identification of a candidate etiologic agent. Virol. J. **5:**88. http://dx.doi.org/10.1186/1743-422X-5-88.